A COMBINED MULTI-TEMPORAL INSAR METHOD INCORPORATING PERSISTENT SCATTERER AND SMALL BASELINE APPROACHES

Andrew Hooper

Nordic Volcanological Centre, University of Iceland, Sturlugata 7, Reykjavik, Iceland

ABSTRACT

InSAR techniques that process data from multiple acquisitions in time enable both the extraction of deformation time series and a reduction of error terms present in single interferograms. There are currently two broad categories of methods that deal with multi-temporal images: persistent scatterer (PS) methods and small baseline (SB) methods. As they are optimized for different scattering models, the two approaches are complementary. Here, a new algorithm is presented that combines both PS and SB approaches. Combination of the two data sets increases both the number of pixels with useable signal and also increases the SNR for pixels selected by both methods. The new algorithm is applied to ERS data acquired over Eyjafjallajökull volcano in Iceland, which experienced intrusive episodes during 1994 and 1999–2000.

Key words: PSI; SBAS; MT-InSAR.

1. INTRODUCTION

Spaceborne synthetic aperture radar interferometry (InSAR) is a useful tool for measuring surface deformation because of the high spatial resolution achieved and the ability to acquire the data remotely. However, problems due to changes in scattering properties of the Earth's surface with time and look direction limit the applicability of this technique. Where measurement is possible, signal due to displacement of the ground is obscured by variation in atmospheric properties and inaccuracy in satellite orbit and surface elevation determination. *Multi-temporal InSAR* (MT-InSAR) techniques, which involve the processing of multiple acquisitions in time, provide one way to address these issues. Currently, there are two broad categories of MT-InSAR techniques, *persistent scatterer* (PS) methods including those that identify pixels based primarily on their phase variation in time [e.g., 1, 2] and those that use primarily correlation of their phase in space [e.g. 3, 4], and *small baseline* (SB) methods [e.g., 5, 6]. The naming of the categories is inconsistent in that "persistent scatterer" refers to the type of pixel that is identified by the method whereas "small baseline" refers to the methodology of interferogram formation. However, as the names are already well-established, I use them throughout this paper.

In a synthetic aperture radar image, the value for each pixel is the coherent sum of contributions from all scatterers within the associated ground resolution element. Relative movement of these scatterers or change in look or squint angle causes the scatterer contributions to sum differently, an effect known as decorrelation [7]. For ground resolution elements containing a persistent dominant scatterer the phase due to decorrelation varies little with time even if the dimmer scatterers move with respect to the dominant scatterer. Furthermore, the variation is also small when viewed from different look and squint angles. This is the principle behind a PS pixel. For resolution elements containing no dominant scatterer, on the other hand, phase variation due to decorrelation is often large enough to obscure the underlying signal. However, by forming interferograms only between images separated by a short time interval the decorrelation in time is minimized, and for some resolution elements may be small enough that the underlying signal is still detectable. Furthermore, if the difference in look and squint angle between each pair of images is also not too large, the corresponding geometric and rotational decorrelation can be reduced by band-pass filtering in range and azimuth [8]. Pixels whose phase when filtered decorrelates little over short time intervals, which I refer to as slow-varying filtered phase (SFP) pixels, are the targets of SB methods. Note that for pixels dominated by a single scatterer, the effect of range and azimuth filtering may be to increase decorrelation due to the coarsening of the resolution. Nevertheless, the decorrelation is often still low enough for some PS pixels that they also qualify as SFP pixels. Thus SFP pixels and PS pixels form two distinct, but overlapping, sets of pixels.

There has been some debate about the relative merits of PS and SB approaches. However, as they are optimized for different models of ground scattering, the two approaches are in fact complementary, at least in the usual case where a data set contains pixels with a range of scattering characteristics. Here I present a new algorithm that combines both PS and SB approaches to maximize the spatial coverage of useable signal. Improvement of the spatial coverage is important not only because it increases the resolution of any deformation signal, but also because it allows for more reliable estimation of integer

phase-cycle ambiguities present in the data. For PS selection I use the method described in [9] and for the SB processing I use a new algorithm described in this paper. After pixel selection, the two data sets are combined and further processing is performed on the combined data set to isolate the deformation signal.

For validation of the approach, I apply the algorithm to Eyjafjallajökull volcano in Iceland, which experienced intrusive episodes during 1994 and 1999 – 2000 [10].

2. PERSISTENT SCATTERER PROCESSING

Interferograms optimized for PS analysis are formed, and PS pixels identified as described in [9]. In order to process large regions on computers with an arbitrary amount of memory, interferograms are split into a number of overlapping patches in range and azimuth. Each patch is then processed independently to identify PS pixels. Once identified, PS pixels from all patches are combined.

3. SMALL BASELINE PROCESSING

Standard SB methods [5, 6] work with interferograms that are first multilooked and then individually phase-unwrapped. However, the processing of multiple acquisitions together offers the potential to process at the highest possible resolution, enabling identification of isolated SFP pixels that are surrounded by pixels that completely decorrelate. Lanari et al. [11] have implemented a method to first identify multi-looked SFP pixels that are then used to identify single-look SFP pixels in a further step. The method I describe here differs in that it operates on single-look images to identify single-look SFP pixels directly.

3.1. Small Baseline Interferograms

Small baseline methods seek to minimize the separation in time and Doppler frequency range of acquisition pairs, in order to maximize the correlation of the interferograms formed. I select image pairs whose perpendicular, temporal and Doppler separation are below threshold values, which depend on data availability for the specific application and expected rate of decorrelation for the given terrain, ensuring that the resultant network of image-pairs contains no isolated clusters (Figure 1). The interferograms are formed by recombination of the resampled SLC images from the PS processing, first filtering in azimuth to exclude non-overlapping Doppler spectrum and in range to reduce the effects of geometric decorrelation. The geometric phase to be subtracted for each small baseline interferogram is calculated as the difference between the relevant single-master interferograms for both the flat-Earth and topographic phase.

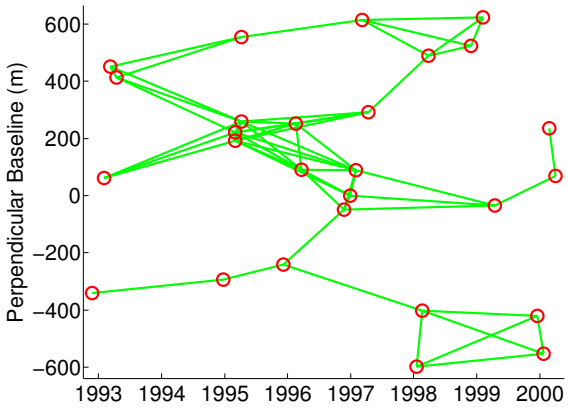

Figure 1. Baseline plot. Circles represent images and lines represent the SB interferograms formed. Perpendicular baseline is with respect to the master image used in the PS processing. Doppler separation for the image-pairs is not shown, but in most cases is less than 100 Hz, with a maximum value of 720 Hz.

3.2. SFP Pixel Selection

Computational burden is reduced by selecting a subset of candidate pixels that is expected to include almost all SFP pixels, through analysis of amplitudes as described in [12]. SFP pixels are identified amongst the candidate pixels in same way as for PS pixels [9]. This involves estimating the spatially-correlated terms by bandpass filtering and the spatially-uncorrelated look angle error term through its correlation with perpendicular baseline. Subtraction of these two estimates leaves an estimate of the decorrelation term which is then characterized in terms of a measure similar to coherence magnitude,

$$\gamma_x = \frac{1}{N}\left|\sum_{i=1}^{N}\exp\{\sqrt{-1}(\psi_{x,i} - \widetilde{\psi}_{x,i} - \Delta\widehat{\phi}^{u}_{\theta,x,i})\}\right|, \quad (1)$$

where $\psi_{x,i}$ is the wrapped phase of pixel x in the ith interferogram, $\widetilde{\psi}_{x,i}$ is the estimate of the spatially-correlated part of $\psi_{x,i}$, $\widehat{\phi}^{u}_{\theta,x,i}$ is the estimate of the spatially-uncorrelated look angle error term and N is the number of interferograms. A threshold value of γ_x for selection is calculated for each pixel based on the percentage of misidentified SFP pixels that is permissible for the specific application.

4. COMBINED DATA SET PROCESSING

Because phase is measured modulo 2π rad, integer phase-cycle ambiguities must be estimated in order to derive the deformation field, a process known as *phase-unwrapping*. The problem of phase-unwrapping is inherently non-unique, but increasing the spatial sampling

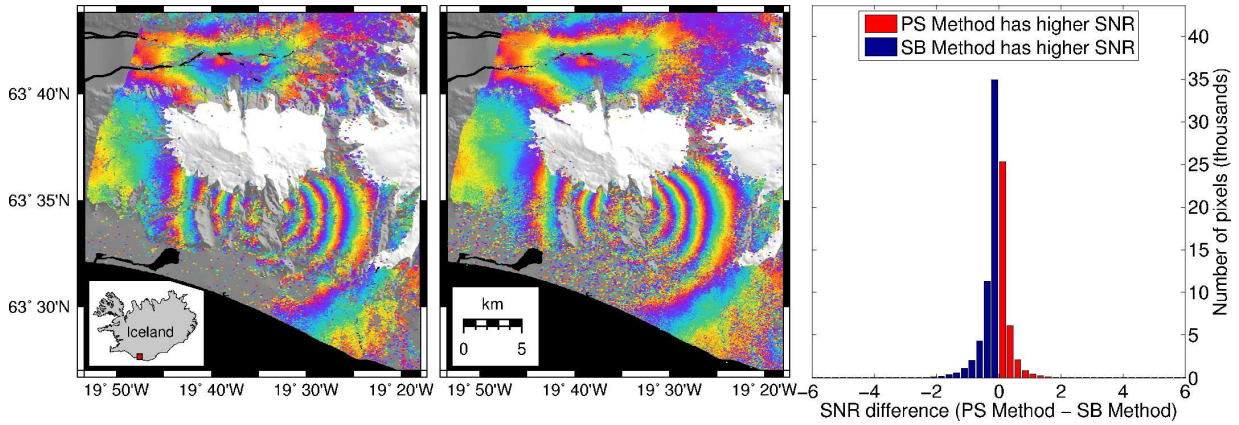

Figure 2. Comparison of pixels on and around Eyjafjallajökull volcano selected by different methods. Left, pixels selected by the PS method [9] and middle, pixels selected by the SB method described in this paper. The pixels are plotted on topography in shaded relief, with white representing the approximate area of permanent ice cover. The location of the area analyzed is shown left inset. 27 images were used in the analysis although only one interferogram is shown here, which covers 27 June 1997 to 10 October 1999. Each color fringe represents 2.8 cm of displacement in the line-of-sight and in both cases the phase of the selected pixels has been filtered using an adaptive phase filter [13]. Right is a comparison of SNR for pixels that are selected by both methods.

reduces the chances of spatial aliasing and thereby increases the chances of success. The PS and SB data sets are therefore combined before this step to maximize the reliability of the unwrapped phase. In order to achieve this, I calculate the equivalent SB interferogram phase, $\psi^{SB}_{x,i}$, for PS pixels by recombination of single-master interferogram phase,

$$\psi^{SB}_{x,i} = W\{\psi^{SM}_{x,s} - \psi^{SM}_{x,m}\} \quad (2)$$

where $\psi^{SM}_{x,s}$ is the single-master phase for the small baseline slave, $\psi^{SM}_{x,m}$ is the single-master phase for the small baseline master, and $W\{\cdot\}$ is the wrapping operator. I re-estimate γ_x (Eq. 1) for PS pixels from the resulting SB interferogram phase. This is usually lower than the value calculated from the single-master interferogram phase, where the master contribution to the decorrelation term is present in every interferogram and does not therefore contribute to the variation. Phase-unwrapping of SB interferograms, which cover short time intervals, as opposed to single-master interferograms has the added advantage of reducing spatial-aliasing in the case of high deformation rates.

A combined data set of SB interferogram phase is created from both PS and SFP pixels. When a pixel occurs in both data sets, a weighted mean value for the phase is calculated by summing the complex signal from both data sets, with the amplitude of each set to an estimate of the signal-to-noise ratio (SNR) for the pixel in that data set. The SNR is estimated as [14]

$$\widehat{SNR} = \frac{1}{\gamma_x^{-1} - 1}. \quad (3)$$

4.1. Phase-Unwrapping

The processing of multiple acquisitions together offers the potential to unwrap the phase more robustly in three dimensions, the third dimension being that of time. The phase of the combined data set is first corrected using the estimate of spatially-uncorrelated look angle error calculated in the selection step for each individual data set. The phase is then unwrapped in a two-step approach. First, a smoothly-varying function in time is found for each pair of neighbouring pixels that minimises the wrapped phase residual between the phase predicted by this function for the small baseline interferograms and the wrapped phase data. Second, this function is used to calculate a probability density function for each pair of pixels in each small baseline interferogram, from which cost functions are calculated and input into the optimisation routines of snaphu [15] to unwrap the phase of each interferogram. The method is described more fully in [16].

4.2. Time Series Inversion

In order to form a time series of phase change for each pixel, the unwrapped phase of the SB interferograms must be inverted. Beraradino et al. [5] perform the inversion using singular value decomposition, imposing an extra minimum-norm constraint. As there are no isolated clusters of interferograms in my analysis, this extra constraint is not required and I invert the unwrapped phase in a least-squares fashion, similar to [6]. The model phase retrieved is then the phase of each pixel relative to an arbitrary reference pixel and master image. To check that the phase for all SB interferograms contributing to each final single-master interferogram is consistent, I calculate the residual phase between the SB interferograms and

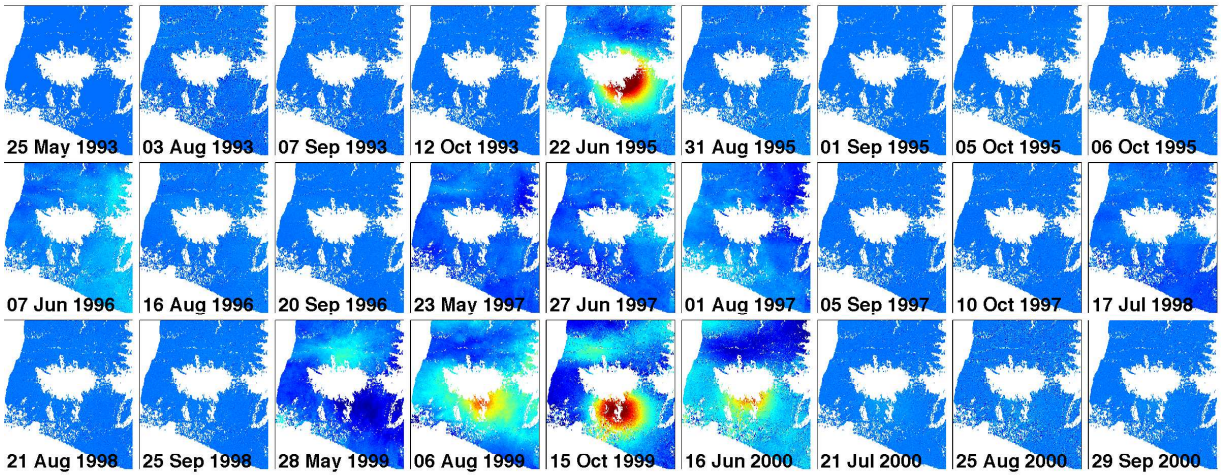

Figure 3. Time series of line-of-sight displacement for Eyjafjallajökull volcano from combined MT-InSAR method. Each image represents the incremental displacement since the time of the previous image, with reference to pixels in the north-west corner. Maximum displacement towards the satellite (red) is 14 cm. Spatially-correlated nuisance terms have been estimated and removed by spatial and temporal filtering following [9], except for the 1999 images, where the temporal sampling with regard to the change in deformation rate is not high enough to separate these terms from deformation.

the phase predicted by the model single-master interferograms. Residuals of up to 2π are expected for individual pixels, due to local unwrapping errors, but any spatially-correlated residuals imply systematic phase-unwrapping errors. If this is the case, problem interferograms are identified and either their phase is unwrapped more carefully, or they are dropped from the inversion when the redundancy of the SB interferograms allows.

5. APPLICATION TO EYJAFJALLAJÖKULL

I applied the combined multi-temporal InSAR method to 27 images acquired by ERS-1 and ERS-2 satellites over Eyjafjallajökull volcano between May 1993 and September 2000 (Figure 1). The same selection threshold, permitting 1% of pixels to have random phase, was used for both methods. Using the PS method 177,000 PS pixels were identified, whereas with the SB method 659,000 SFP pixels were identified. This implies that there are more ground resolution elements containing a distribution of semi-stable scatterers than those dominated by a single scatterer. Of the selected pixels, 133,000 were selected by both methods, implying that the true phase characteristics of these pixels lie somewhere between the two scattering models for which the two methods are optimized. Raising the selection threshold for PS pixels to 10% led to a greater proportion of the pixels being selected by the PS method only, indicating that PS pixels are not merely a subset of SFP pixels. Figure 2 (right) shows the difference in SNR (Eq. 3) between the two methods for the common pixels. For about half of these pixels, SNR is higher using the SB method, implying that these pixels are closer to the Gaussian scatterer model and band-pass filtering increases SNR. The other half are presumably closer to the point scatterering model and band-pass filtering apparently decreases their SNR. The wrapped phase of pixels selected by both methods for a single time interval is shown in Figure 2 (left and middle). Both methods find isolated pixels, even in the ice cap region, where nunataks project through.

Results from the combined method are shown in Figure 3. There were two intrusive episodes, the first of which occured in 1994 and the second of which began in 1999 and ended in early 2000 [10]. The deformation caused by the two episodes is clearly centered at different locations, which was also the conclusion from conventional InSAR analysis [10]. The overall deformation pattern for each episode is more even than deduced from conventional InSAR, however, due to the removal of digital elevation model and atmospheric artifacts, and more accurate phase-unwrapping in the time series analysis.

6. CONCLUSIONS

Using the new SB method presented here, it is possible to extract the deformation signal, at the highest possible resolution, from pixels with slow-varying filtered phase. When combined with pixels identified by the PS method, the result is an increase in the number of pixels with useable signal and higher SNR for pixels selected by both approaches. The combined multi-temporal InSAR algorithm therefore enables extraction of the deformation signal at more points and more reliably than can either method alone. The combined method was applied to Eyjafjallajökull volcano, and a time series for the displacement field was retrieved that includes two intrusion episodes.

ACKNOWLEDGMENTS

I thank Ramon Hanssen for comments. ERS data were provided by the European Space Agency. Focused SAR images were produced using the ROI_PAC software package developed by the Jet Propulsion Laboratory. Interferometric processing was partially performed using the Doris software package developed by Delft University of Technology. This research was supported by the European Sixth Framework Program VOLUME project.

REFERENCES

[1] A. Ferretti, C. Prati, and F. Rocca. Permanent scatterers in SAR interferometry. *IEEE Trans. Geosci. and Remote Sens.*, 39(1):8 – 20, 2001.

[2] B. M. Kampes. *Displacement Parameter Estimation Using Permanent Scatterer Interferometry*. PhD thesis, Delft University of Technology, 2005.

[3] A. Hooper, H. Zebker, P. Segall, and B. Kampes. A new method for measuring deformation on volcanoes and other natural terrains using InSAR persistent scatterers. *Geophys. Res. Lett.*, 31(23), 2004.

[4] M. van der Kooij, W. Hughes, S. Sato, and V. Poncos. Coherent target monitoring at high spatial density: Examples of validation results. *European Space Agency, (Special Publication) ESA SP*, 2006.

[5] P. Berardino, G. Fornaro, R. Lanari, and E. Sansosti. A new algorithm for surface deformation monitoring based on small baseline differential SAR interferograms. *IEEE Transactions on Geoscience and Remote Sensing*, 40(11):2375 – 83, 2002.

[6] D. A. Schmidt and R. Bürgmann. Time-dependent land uplift and subsidence in the Santa Clara valley, California, from a large interferometric synthetic aperture radar data set. *Journal of Geophysical Research*, 108(B9):2416 – 28, 2003.

[7] H. A. Zebker and J. Villasenor. Decorrelation in interferometric radar echoes. *IEEE Trans. Geosci. Remote Sens.*, 30(5):950 – 9, 1992.

[8] F. Gatelli, A. M. Guamieri, F. Parizzi, P. Pasquali, C. Prati, and F. Rocca. The wavenumber shift in SAR interferometry. *IEEE Trans. Geosci. Remote Sens.*, 32(4):855 – 865, 1994.

[9] A. Hooper, P. Segall, and H. Zebker. Persistent scatterer InSAR for crustal deformation analysis, with application to Volcán Alcedo, Galápagos. *J. Geophys. Res.*, 112(B07407), 2007.

[10] R. Pedersen and F. Sigmundsson. Temporal development of the 1999 intrusive episode in the Eyjafjallajökull volcano, Iceland, derived from InSAR images. *Bull. Volcanol.*, 68:377–393, 2006.

[11] R. Lanari, O. Mora, M. Manunta, J. J. Mallorqui, P. Berardino, and E. Sansosti. A small-baseline approach for investigating deformations on full-resolution differential SAR interferograms. *IEEE Trans.Geosci. Remote. Sens.*, 42(7):1377–1386, 2004.

[12] A. Hooper. A multi-temporal InSAR method incorporating both persistent scatterer and small baseline approaches. *Geophys. Res. Lett.*, in prep.

[13] R. M. Goldstein and C. L. Werner. Radar interferogram filtering for geophysical applications. *Geophys. Res. Lett.*, 25(21):4035 – 8, 1998.

[14] D. Just and R Bamler. Phase statistics of interferograms with applications to synthetic-aperture radar. *Applied Optics*, 33(20):4361–4368, 1994.

[15] C. W. Chen and H. A. Zebker. Two-dimensional phase unwrapping with use of statistical models for cost functions in nonlinear optimization. *Journal of the Optical Society of America A (Optics, Image Science and Vision)*, 18(2):338 – 51, 2001.

[16] A. Hooper. Statistical cost approach to unwrapping the phase of multiple radar interferograms. *IEEE Transactions on Geoscience and Remote Sensing*, in prep.